Low-Profile Wideband Microstrip Antenna Based on Multiple Modes With Partial Apertures

Wenxing An, Shenrong Li, Wangyu Sun, and Yue Li, *Senior Member, IEEE*

***Abstract*—In this letter, a low-profile microstrip antenna is presented for wideband requirement for both -10 dB $|S_{11}|$ and 3 dB gain bandwidth. Multiple modes with partial apertures are introduced to broaden the bandwidth within a relatively low profile. The working mechanism of the proposed antenna is analyzed, and the designed antenna has an impedance bandwidth of 57.3% (from 2.94 to 5.3 GHz), covering the frequency bands of fifth generation between 3 and 5 GHz with dimensions of $1.29\lambda_0 \times 1.01\lambda_0 \times 0.044\lambda_0$, where λ_0 is the free-space wavelength of 4 GHz. The antenna prototype is fabricated, and the measured results are in good agreement with the simulation ones. The measured average gain is 5.26 dBi, and the radiation patterns remain stable in the target band with low cross-polarization levels at both principle planes.**

***Index Terms*—Low-profile wideband antennas, microstrip antennas, multiple modes, periodically slot-loaded structures.**

I. Introduction

As THE next generation of wireless mobile communication system, the fifth generation (5G) accelerates its technical progress, and the experimental networks are being deployed in some pilot cities. To accommodate the sharp growing of wireless transfer rate, micro base station antennas are in large demand for 5G system, expected to be thinner in profile, easy for integration and low-cost for large-scaled deployment. In the past few years, most countries have announced their spectrum plans for 5G services [1]–[5]. Taking account of different sub-6 GHz bands for 5G all over the world, it is much appreciated to achieve a wideband but low-profile antenna covering the wide frequency band from 3 to 5 GHz.

Manuscript received April 9, 2019; revised May 6, 2019; accepted May 6, 2019. Date of publication May 15, 2019; date of current version July 3, 2019. This work was supported in part by the National Natural Science Foundation of China under Grant 61701339, in part by the AoShan Talents Cultivation Program Supported by Qingdao National Laboratory for Marine Science and Technology under Grant 2017ASTCP-OS03, in part by the Leading Talents of Guangdong Province Program under Grant 2016LJ06D557, and in part by Guangdong Yangfan Plans to Introduce Innovative Entrepreneurship Team Project 2016YT04G420. *(Corresponding author: Yue Li.)*

W. An and S. Li are with the Tianjin Key Laboratory of Imaging and Sensing Microelectronic Technology, School of Microelectronics and Qingdao Institute of Ocean Engineering, Tianjin University, Tianjin 300072, China, with the Joint Laboratory for Ocean Observation and Detection, Qingdao National Laboratory of Marine Science and Technology, Qingdao 266237, China, with the Tianjin Engineering Center of Integrated Circuit and Computing Systems, Tianjin 300072, China, and also with Tianjin International Joint Research Center of Internet of Things, Tianjin 300072 China (e-mail: anwenxing@126.com; 1985741303@qq.com).

W. Sun and Y. Li are with the Department of Electronic Engineering, Tsinghua University, Beijing 100084, China (e-mail: sunwy16@mails.tsinghua.edu.cn; lyee@tsinghua.edu.cn).

Digital Object Identifier 10.1109/LAWP.2019.2917077

Low-profile and wideband antenna is an attractive research topic in recent years, and many technologies have been studied and employed. Bandwidths of 14% and 31% were realized by H- and U-slot loaded patch antennas [6], [7]. Utilizing meandering and L-shaped probes, the bandwidth was improved to be ∼35% [8], [9]. Then, a bandwidth of 40% was reported by stacked and E-shaped antennas [10], [11]. After that, EM-dipole antenna was proposed with identical radiation patterns at two principle planes [12], [13], and wideband performance of more than 50% was obtained. Based on artificial magnetic conductor surface, wideband patch antenna was presented in [14] with a relative bandwidth of 55%. A hybrid design employing patch and slot structures was discussed with the measured bandwidth of 50% in [15] and [16]. Although all the above-mentioned designs have good performances, they all have a relatively large profile of more than $0.1\lambda_0$.

Recently, a metamaterial-based broadband low-profile mushroom antenna was presented in [17] with TM_{10} and antiphase TM_{20} modes. Circularly polarized antenna array using a thin metasurface structure was proposed in [18]. Formed by a diamond-slotted patch, a low-profile and wideband metasurface antenna was reported in [19], and a low profile of $0.07\lambda_0$ was achieved with the bandwidth of 31%. A nonuniform tapered metasurface antenna with monopole-like radiation pattern was investigated in [20]. Dual-band performance was discussed in [21] with rectangular mushroom-like metasurface. The latest progress of this metasurface antenna has realized a reduced radiating aperture with a profile of $0.06\lambda_0$ and similar bandwidth of 30% [22]. For a universal 5G base station antenna, a lower profile and wide band of at least 50% are preferred for the sub-6 GHz band with stable performance and low cost.

For a low-profile antenna, multiple modes are an effective way to achieve a wideband performance based on partial or total aperture. As an example in [23], the feeding strips and elliptical patches resonate at different frequency with different radiation apertures. Another design is shown in [24]: The feeding strips, elliptical loop, and inner patches functions at three different resonant frequency points, but the feeding strips and inner patches only employ a relatively small and partial aperture at higher frequency band. For the proposed antenna structure, there are 20 small patches divided by several slots to form the overall radiating aperture, fed by an asymmetric dual-aperture-coupling structure. Based on this configuration, it is possible to stimulate some resonant modes with partial apertures.

In this letter, multiple modes with partial aperture are coupled to enhance the bandwidth by properly designing the radiation

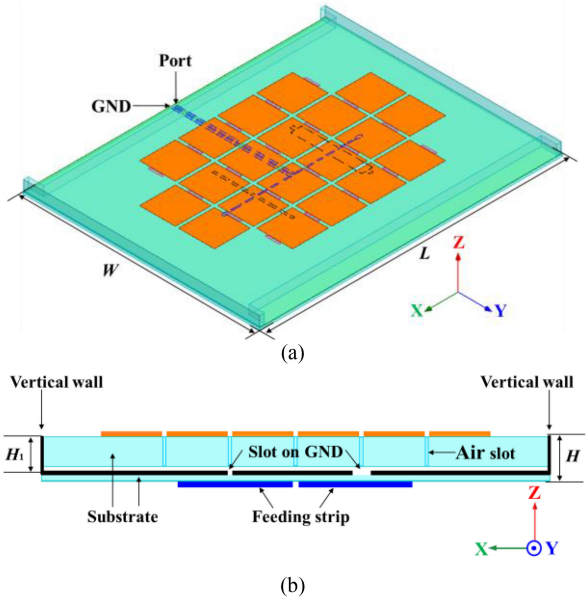

Fig. 1. Structure of the proposed microstrip antenna. (a) Perspective view. (b) Side view in xz plane.

and feeding structures. A prototype of the proposed antenna is constructed and tested. The measured impedance bandwidth from 2.94 to 5.3 GHz is realized with a low profile of $0.044\lambda_0$. Good radiation performances are obtained including low cross-polarization levels and stable gain within the required band.

II. Antenna Structure and Analysis

A. Antenna Structure

The antenna structure is depicted in Figs. 1 and 2. It is observed that the proposed microstrip antenna is based on periodical structure, which is placed at the center of a ground with a dimension of 97×76 mm^2. It contains two layers of FR4 substrates with the thicknesses of 3 and 0.7 mm, separated by an air gap of 0.25 mm. The measured relative dielectric constant of the FR4 is 3.85 with the loss tangent of 0.0185 between 3 and 5 GHz. The antenna height above the ground is 3.25 mm, and the corresponding profile is $\sim 0.044\lambda_0$ (λ_0 is the free-space wavelength of 4 GHz). Detailed antenna sizes are listed in Table I. The periodically arranged small patches and slots act as the main radiation aperture, and there are totally 20 small patches printed on the top of the upper FR4 substrate, as shown in Fig. 2(a). The patches have the sizes of L_1 and W_1, with the distances of G_1 and G_2 among each other. To decrease the effective relative dielectric constant for wideband performance, 20 air slots with the sizes of S and S_1 are carved on the FR4 substrate among these small patches. The feeding structure is printed on the bottom FR4 substrate, as shown in Fig. 2(b).

Dual-aperture-coupling mechanism is adopted for the excitation, including a ground plane, a parallel transmission line, and aperture-coupling structures. As shown in Fig. 2(b), one strip of the parallel transmission line is soldered with the inner conductor of a 50 Ω SMA connector; the other strip is connected to the ground plane through three vias with a diameter of 0.375

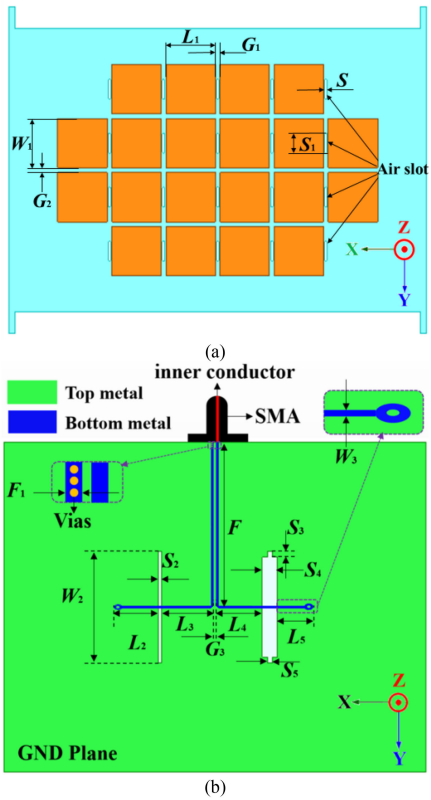

Fig. 2. Geometry of the proposed microstrip antenna. (a) Top layer. (b) Bottom layer.

TABLE I
Antenna Parameters (mm)

Para.	L	L_1	L_2	L_3	L_4	L_5	W	W_1
Value	97	11.5	9.62	12.1	10.72	8.035	76	11.5
Para.	W_2	W_3	F	F_1	G_1	G_2	G_3	H
Value	25.8	0.42	37.79	0.675	1.06	1.06	0.18	3.95
Para.	H_1	S	S_1	S_2	S_3	S_4	S_5	
Value	3.25	0.62	4.62	0.73	1.45	3.5	1.1	

mm and separation distance of 0.15 mm. The outer conductor of the SMA connector and the ground plane are soldered together. Two slots with different widths are carved on the ground plane. The widths of two slots are modified to construct the multiple modes with partial aperture at higher frequency. Two vertical metallic walls are added along polarization direction to provide an electromagnetic shield from nearby circuits, as shown in Fig. 1(b). To improve the impedance matching, two hollow ellipses are integrated at the end of the feeding strip from the aperture coupling structure with the outer main and subdiameters of 1.8 and 1.125 mm, and the inner main and subdiameters of 0.8 and 0.5 mm, respectively.

B. Antenna Analysis

To clarify the wideband performance, multiple modes with partial apertures are introduced, and Z-parameters are plotted in Fig. 3. By manipulating the periodical small patches and asymmetrical dual-aperture-coupling structure, three resonant frequencies are formulated within the target band at 3.15, 3.79,

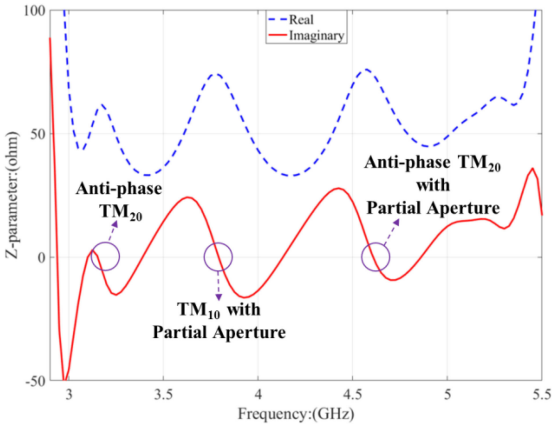

Fig. 3. Simulated Z-parameters of the antenna over the passband.

and 4.6 GHz, respectively. The simulated E-field distributions are plotted at three resonant frequencies in Fig. 4.

At the lower frequency of 3.15 GHz, all the 20 small patches are excited. As the frequency increases, the radiation aperture starts to decrease. It is observed from Fig. 4 that the effective radiation aperture has shifted to the right side with reduced radiation area as frequency increases. The phenomenon is caused by the asymmetric feeding structure. The feeding structures can provide a balanced feed at lower frequency, but unbalanced feed at higher band. It is obvious in Fig. 4(b) and (c) that only partial apertures are excited at higher frequencies, and more energy is concentrated at the area near the right slot.

To clarify the working mechanism, the E-field distributions are investigated. It is noticed in Fig. 4(a) that the direction of E-field vector has switched three times along the polarization direction; it is the antiphase TM_{20} mode at 3.15 GHz. In Fig. 4(b), the E-field vector direction has changed only once along the polarization direction with reduced radiation area; it is the TM_{10} mode at 3.79 GHz based on partial aperture. In Fig. 4(c), the E-field vector direction has varied three times; it is the antiphase TM_{20} mode at 4.6 GHz with partial aperture.

Two additional elements have been added at each side along the polarization direction, so it is necessary to investigate its influence on the antenna radiation performance. The antenna gains with and without side elements are plotted in Fig. 5. It is observed that these side elements can help to augment the antenna gain, especially at higher frequency band. This can also be verified from Fig. 4. It is observed that there are more energy distributions near the side elements at higher frequency points, but less energy distributions at lower frequency. In order to improve the impedance matching of the low-profile microstrip antenna, rows of air slots are introduced by removing partial substrate [25]. The air slot can decrease the effective relative dielectric constant, leading to a lower Q-factor. Thus, it can help to improve the impedance matching and the S-parameter.

III. Experimental Verification

The proposed antenna is numerically simulated using the software of High Frequency Structure Simulator. To verify the antenna design, a prototype is fabricated and shown in Fig. 6.

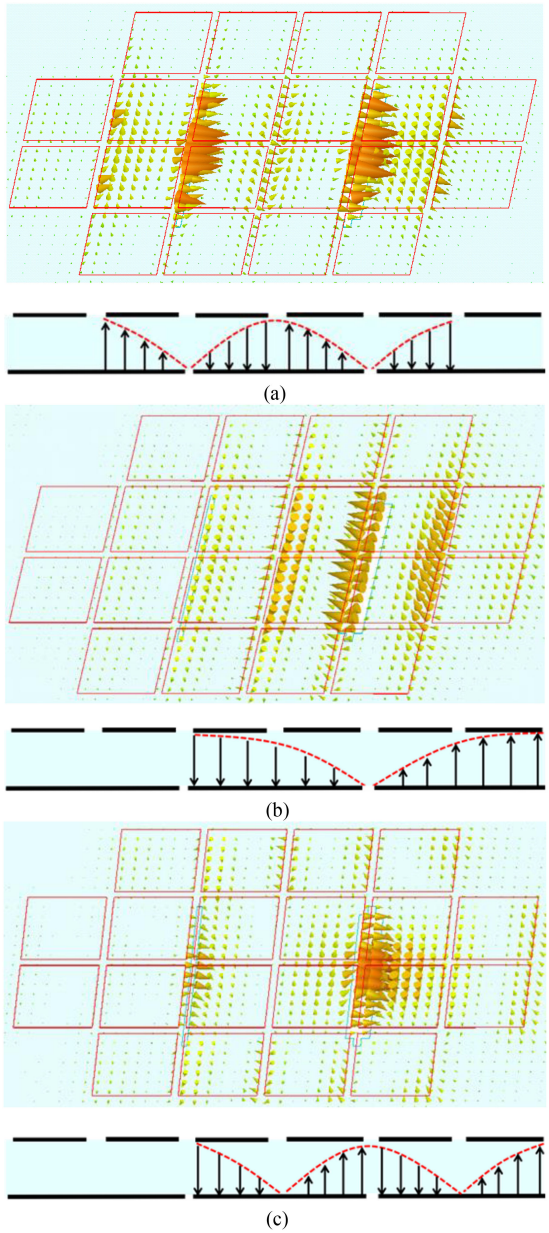

Fig. 4. Snapshots of E-field distributions on horizontal plane ($z = 1.5$ mm) and vertical plane ($y = 0$ mm) at different resonant frequencies. (a) 3.15 GHz. (b) 3.79 GHz. (c) 4.6 GHz.

The antenna prototype is measured using the Agilent E5071C network analyzer and an anechoic chamber. The simulated and tested S-parameter and gain results are depicted in Fig. 7. The measured 10 dB bandwidth is from 2.94 to 5.3 GHz with a relative bandwidth of 57.3%, and there are more than three resonant frequency points within the passband. Measured gain at the normal direction has a variation of 3 dB between 3.08 and 5.22 GHz in Fig. 7, and it is obvious that the target band from 3.1 to 5 GHz is fully covered. Broadside radiation patterns are obtained, and the patterns at 3.5 and 4.5 GHz are shown in Fig. 8. It is observed that the simulated and tested copolarization results almost overlap with each other, whereas the tested cross-polarization levels are below -18 dB.

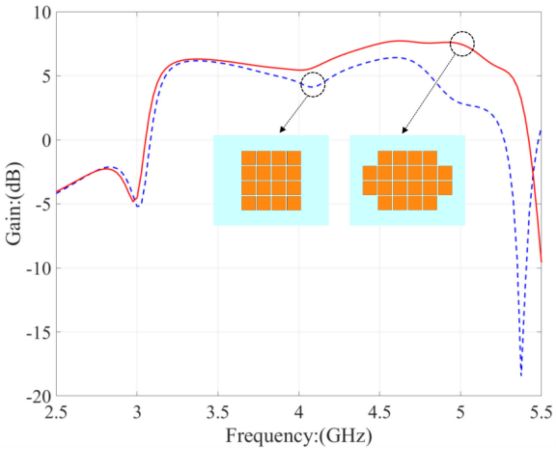

Fig. 5. Simulated antenna gains with and without side elements.

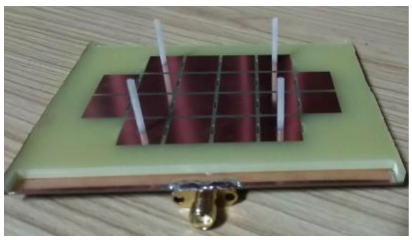

Fig. 6. Prototype of the proposed microstrip antenna.

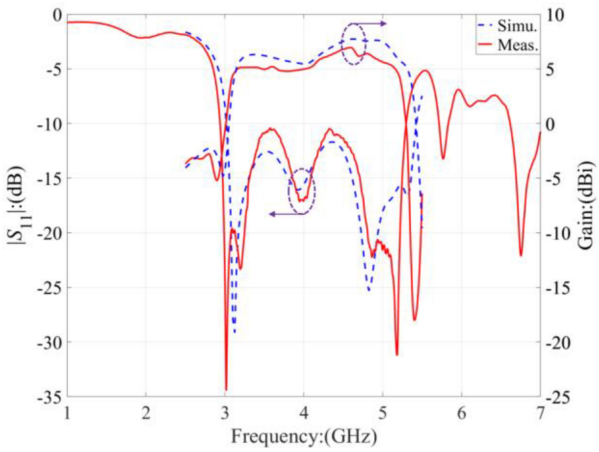

Fig. 7. Measured and simulated *S*-parameter and gain results of the proposed microstrip antenna.

To further understand the proposed antenna, comparisons are conducted between this and other published works in Table II. The initial mushroom antenna has a bandwidth of 25% and a profile of $0.06\lambda_0$ using fundamental and high-order modes [17]. The impedance band was improved to be ~30% [19] with reduced aperture [22]. An omnidirectional pattern was reported with a relative bandwidth of 33.1% [20]. A dual-band performance was achieved with a low profile of $0.034\lambda_0$ and a relatively narrow frequency band [21]. This letter has achieved wider impedance matching and 3 dB gain bandwidths simultaneously; both are more than 50% with a lower profile of $0.044\lambda_0$. Compared with the others, multiple modes with partial apertures are adopted for low-profile and wideband design.

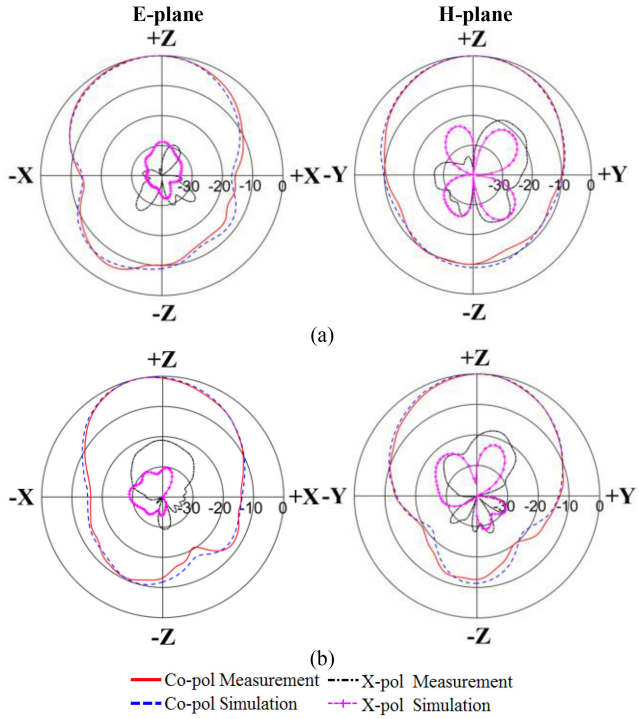

Fig. 8. Simulated and measured radiation patterns of the proposed antenna. (a) 3.5 GHz. (b) 4.5 GHz.

TABLE II
COMPARISON OF THE PROPOSED ANTENNA WITH EXISTING DESIGNS

Ref.	Bandwidth (%)	Size (λ_0 at center freq.)	3-dB Gain Bandwidth (%)	Mode
[17]	25	1.1×1.1×0.06	32.9	TM_{10} Anti-TM_{20}
[19]	31	1.78×1.78×0.07	30.6	Characteristic mode
[20]	33.1	1.29×1.29×0.06	36.3	$TM_{01,02}$
[21]	25.8 (low band) 15.1 (high band)	0.264×0.26×0.034 0.59 ×0.54×0.076	37 31.9	0th-order $TM_{10,20}$
[22]	30	0.46×0.46×0.06	34.2	N.A.
This work	57.3	1.29×1.01×0.044	51.6	TM_{10}, Anti-TM_{20}

IV. CONCLUSION

A low-profile and wideband microstrip antenna is proposed for the 5G base station. The multiple modes with partial apertures are investigated for wideband performance. Using TM_{10} and antiphase TM_{20} modes with partial apertures, multiple modes are conducted, and a wideband performance of 57.3% has been achieved from 2.94 to 5.3 GHz. Furthermore, a lower profile of $0.044\lambda_0$ has been realized based on the periodically slotted microstrip antenna. Satisfactory radiation performances are obtained with low cross-polarization levels. Because of these favorable features, this low-profile and wideband antenna exhibits potential usage for 5G base station.

REFERENCES

[1] J. Barrett, "5G spectrum bands," Feb. 2017. [Online]. Available: https://gsacom.com/5g-spectrum-bands/

[2] 4G LTE Mall, "5G frequency bands allocation globally," Jul. 2018. [Online]. Available: https://www.4gltemall.com/blog/5g-frequency-bands-allocation-globally/

[3] Q. Wu, P. Liang, and X. Chen, "A broadband ±45° dual-polarized multiple-input multiple-output antenna for 5G base stations with extra decoupling elements," *J. Commun. Inf. Netw.*, vol. 3, no. 1, pp. 31–37, Mar. 2018.

[4] Y. Li, C. Y. D. Sim, Y. Luo, and G. Yang, "Multiband 10-antenna array for sub-6 GHz MIMO applications in 5-G smartphones," *IEEE Access*, vol. 6, pp. 28041–28253, 2018.

[5] Y. Li, C. Y. D. Sim, Y. Luo, and G. Yang, "12-port 5G massive MIMO antenna array in sub-6 GHz mobile handset for LTE bands 42/43/46 applications," *IEEE Access*, vol. 6, pp. 344–354, 2018.

[6] C. Y. D. Sim, C. C. Chang, and J. S. Row, "Dual-feed dual-polarized patch antenna with low cross polarization and high isolation," *IEEE Trans. Antennas Propag.*, vol. 57, no. 10, pp. 3321–3324, Oct. 2009.

[7] M. Khan and D. Chatterjee, "Characteristic mode analysis of a class of empirical design techniques for probe-fed, U-slot microstrip patch antennas," *IEEE Trans. Antennas Propag.*, vol. 64, no. 7, pp. 2758–2770, Jul. 2016.

[8] H. W. Lai and K. M. Luk, "Design and study of wide-band patch antenna fed by meandering probe," *IEEE Trans. Antennas Propag.*, vol. 54, no. 2, pp. 564–571, Feb. 2006.

[9] C. L. Mak, K. M. Luk, K. F. Lee, and Y. L. Chow, "Experimental study of a microstrip patch antenna with an L-shaped probe," *IEEE Trans. Antennas Propag.*, vol. 48, no. 5, pp. 777–783, May 2000.

[10] B. L. Ooi, S. Qin, and M. S. Leong, "Novel design of broad-band stacked patch antenna," *IEEE Trans. Antennas Propag.*, vol. 50, no. 10, pp. 1391–1395, Oct. 2002.

[11] F. Yang, X. X. Zhang, X. Ye, and Y. Rahmat-Samii, "Wide-band E-shaped patch antennas for wireless communications," *IEEE Trans. Antennas Propag.*, vol. 49, no. 7, pp. 1094–1100, Jul. 2001.

[12] K. M. Luk and H. Wong, "A new wideband unidirectional antenna element," *Int. J. Microw. Opt. Technol.*, vol. 1, no. 1, pp. 35–44, 2006.

[13] H. W. Lai and H. Wong, "Substrate integrated magneto-electric dipole antenna for 5G Wi-Fi," *IEEE Trans. Antennas Propag.*, vol. 63, no. 2, pp. 870–874, Feb. 2015.

[14] N. M. Mohamed-Hicho, E. Antonino-Daviu, M. Cabedo-Fabrés, and M. Ferrando-Bataller, "A novel low-profile high-gain UHF antenna using high-impedance surfaces," *IEEE Antennas Wireless Propag. Lett.*, vol. 14, pp. 1014–1017, 2015.

[15] J. Zhang and Z. Shen, "Compact and high gain UHF/UWB RFID reader antenna," *IEEE Trans. Antennas Propag.*, vol. 65, no. 10, pp. 5002–5010, Oct. 2017.

[16] J. Zhang and Z. Shen, "Dual-band shared-aperture UHF/UWB RFID reader antenna of circular polarization," *IEEE Trans. Antennas Propag.*, vol. 66, no. 8, pp. 3886–3993, Aug. 2018.

[17] W. Liu, Z. N. Chen, and X. Qing, "Metamaterial-based low-profile broadband mushroom antenna," *IEEE Trans. Antennas Propag.*, vol. 62, no. 3, pp. 1165–1172, Mar. 2014.

[18] K. L. Chung, S. Chaimool, and C. Zhang, "Wideband subwavelength profile circularly polarized array antenna using anisotropic metasurface," *Electron. Lett.*, vol. 51, no. 18, pp. 1403–1405, Sep. 2015.

[19] F. H. Lin and Z. N. Chen, "Low-profile wideband metasurface antennas using characteristic mode analysis," *IEEE Trans. Antennas Propag.*, vol. 65, no. 4, pp. 1706–1713, Apr. 2017.

[20] G. Feng, L. Chen, X. Xue, and X. Shi, "Broadband surface-wave antenna with a novel nonuniform tapered metasurface," *IEEE Antennas Wireless Propag. Lett.*, vol. 16, pp. 2902–2905, 2017.

[21] Z. Wu, L. Li, X. Chen, and K. Li, "Dual-band antenna integrating with rectangular mushroom-like superstrate for WLAN applications," *IEEE Antennas Wireless Propag. Lett.*, vol. 15, pp. 1269–1272, 2016.

[22] W. E. I. Liu, Z. N. Chen, X. Qing, J. Shi, and F. H. Lin, "Miniaturized wideband metasurface antennas," *IEEE Trans. Antennas Propag.*, vol. 65, no. 12, pp. 7345–7349, Dec. 2017.

[23] W. An, Z. Shen, and J. Wang, "Compact low-profile dual-band tag antenna for indoor positioning systems," *IEEE Antennas Wireless Propag. Lett.*, vol. 16, pp. 400–403, 2017.

[24] W. An, Y. Li, H. Fu, J. Ma, W. Chen, and B. Feng, "Low-profile and wideband microstrip antenna with stable gain for 5G wireless applications," *IEEE Antennas Wireless Propag. Lett.*, vol. 17, no. 4, pp. 621–624, Apr. 2018.

[25] S. B. Yeap and Z. N. Chen, "Microstrip patch antennas with enhanced gain by partial substrate removal," *IEEE Trans. Antennas Propag.*, vol. 58, no. 9, pp. 2811–2816, Sep. 2010.